Journal of Materials Chemistry B

ROYAL SOCIETY OF CHEMISTRY

PAPER

View Article Online
View Journal | View Issue

Cite this: J. Mater. Chem. B, 2022, 10, 2649

Sulfobetaine polymers for effective permeability into multicellular tumor spheroids (MCTSs)†

Nobuyuki Morimoto, *[a] Keisuke Ota,[a] Yuki Miura,[a] Heungsoo Shin [bc] and Masaya Yamamoto *[ad]

Received 25th October 2021,
Accepted 13th December 2021

DOI: 10.1039/d1tb02337c

rsc.li/materials-b

Multicellular tumor spheroids (MCTSs) are attractive for drug screening before animal tests because they emulate an *in vivo* microenvironment. The permeability of the MCTSs and tumor tissues towards the candidate drugs is not sufficient even though the drugs can penetrate monolayer cultured cells; therefore, nanocarriers are required to enhance permeability and deliver drugs. In this study, we prepared zwitterionic polymers of sulfobetaine methacrylates and (meth)acrylamides with or without hydroxy groups between the zwitterions to serve as highly permeable nanocarriers. In the sulfobetaine polymers, poly(2-hydroxy-3-((3-methacrylamidopropyl)dimethylammonio)propane-1-sulfonate), P(OH–MAAmSB), the hydroxy group containing methacrylamide polymer exhibited little cytotoxicity and membrane translocation ability against monolayer cultured cells. Moreover, the excellent permeability of the hepatocyte MCTS enabled P(OH–MAAmSB) to permeate it and reach the center region (~325 μm in diameter) at approximately 150 s, although poly(trimethyl-2-methacroyloxyethylammonium), a cationic polymer, penetrated just 1 to 2 layers from the periphery. The superior permeability of P(OH–MAAmSB) might be due to its good solubility and side chain conformation. P(OH–MAAmSB) is a promising nanocarrier with membrane translocation and permeability.

1. Introduction

Cancer is a leading cause of death in every country of the world.[1] One of the difficulties for cancer treatment is that cancer has a wide variety of pathological conditions with intratumor heterogeneity.[2] Although various cancer treatments have been developed,[3,4] selection of the optimized treatment is still difficult against each type of cancer. In addition to surgery and radiation therapy, chemotherapy is the most popular cancer treatment. However, in the development of anticancer drugs, there are mismatches between monolayers cultured *via in vitro* and *in vivo* studies. Monolayer cultured cells are unable to simulate the complexity and dynamic interactions of a tumor microenvironment.[5] Multicellular tumor spheroids (MCTSs) have been in focus over the past few decades to bridge the gap between *in vitro* and *in vivo* tests for drug screening.[6,7] The MCTS is a 3-dimensional spherical cancer cell aggregate that is used in the construction of *in vivo*-like microenvironments that are more realistic than monolayer cultured cells. MCTSs enhance cell–cell interactions and cell–extracellular matrix interactions to upregulate biochemical and mechanical signals;[8] therefore, various techniques have been developed for the preparation of spheroids.[9–11] However, the size of a spheroid is limited to a few hundreds of micrometers because of the lack of oxygen and nutrients supplies, and metabolite excretion. Such microenvironments are similar to tumor environments; nevertheless, the excess induction of necrosis and apoptosis by long-term culture is not preferable for quality and reproducibility in *in vitro* tests. From such a viewpoint, nanocarriers are applicable to drug delivery. The drug permeability and efficacy of nanocarriers have been evaluated using spheroids.[12–15] These reports showed that the smaller size of nanoparticles and the surface charge greatly influenced the permeation into MCTSs. However, these findings are still insufficient for the further development of nanocarriers. If we could obtain nanocarriers that are highly permeable to MCTS, the nanocarriers are expected to be utilized for *in vivo* applications, in addition to accurate high-speed drug screening.

Sulfobetaine polymers are zwitterionic polymers with sulfonate groups as the anionic pair.[16–18] One of the representative sulfobetaine polymers, poly(3-((2-methacryloyloxyethyl) dimethyl-

[a] Department of Materials Processing, Graduate School of Engineering, Tohoku University, 6-6-02 Aramaki-aza Aoba, Aoba-ku, Sendai 980-8579, Japan. E-mail: morimoto@material.tohoku.ac.jp, masaya.yamamoto.b6@tohoku.ac.jp
[b] Department of Bioengineering, Hanyang University, Seoul 04763, Republic of Korea
[c] BK21 FOUR, Education and Research Group for Biopharmaceutical Innovation Leader, Hanyang University, Seoul 04763, Republic of Korea
[d] Graduate School of Medical Engineering, Tohoku University, 6-6-12 Aramaki-aza Aoba, Aoba-ku, Sendai 980-8579, Japan

† Electronic supplementary information (ESI) available. See DOI: 10.1039/d1tb02337c

ammonio)propane-1-sulfonate), P(MASB), is known for its antifouling properties, and there have been many studies on obtaining bioinert surfaces.[19–21] Interestingly, P(MASB) is also known to show upper critical solution temperature (UCST)-type thermoresponsiveness in pure water based on dipole–dipole interactions between the polymer chains.[22–24] However, the thermoresponsiveness disappears under physiological salt conditions because the weak dipole–dipole interaction is replaced by ion–dipole interactions that dissociate the aggregates. Because of the easy synthesis that uses the opening reaction of 1,3-propane sultone or 1,4-butane sultone with ternary amine, various sulfobetaine polymers with zwitterionic moieties in the side chains have been reported; the monomers were designed to have polymerizable groups (methacrylate, methacrylamide, vinyl groups, *etc.*), combinations of cations (ammonium, pyridinium, imidazolium, *etc.*), N-substituents,[25,26] and alkyl chain spacers between zwitterion pairs. Some sulfobetaine polymers have been successfully prepared to control the thermoresponsiveness near physiological conditions by fine tuning the monomer, molecular weight, and composition of the copolymer for biotechnological applications.[27–30] There have been a small number of studies on sulfobetaine polymers that have side chains between the zwitterions.[31,32] Hildebrand *et al.* prepared hydroxy group substituted poly(sulfobetaine methacrylamide), referred to here as P(OH–MAAmSB) and examined the effects of Hofmeister salts on the cloud points of polymer solutions.[27,31] Interestingly, this transition behavior was quite different from that of P(MAAmSB), and P(OH–MAAmSB) showed an opposite temperature shift behavior to that of P(MAAmSB) in the Hofmeister series. In our previous study, we prepared P(MASB-*co*-poly(ethylene glycol)methacrylate), P(MASB-*co*-PEGMA), and found that the polymer showed cellular membrane translocation with controllable localization to mitochondria.[33,34] More recently, we found that anticancer drug-conjugated P(MASB-*co*-PEGMA) can effectively permeate the center of glioblastoma MCTSs (diameter: ~300 μm) within 2 h and exhibit enhanced drug efficacy.[35] We also studied membrane translocation, and reported that a sulfobetaine methacrylate with a pyridinium cation showed cytotoxicity with membrane disruption at 1.0 mg mL^{-1}, although methacrylamide had no significant cytotoxicity.[36] These results indicated that the polymers could more efficiently permeate the MCSTs if the sulfobetaine structures were fine-tuned. In this study, we prepared sulfobetaine polymers by focusing on the main chain structure (methacrylate or (meth)acrylamide) and introducing hydroxy groups between the zwitterion pair (Fig. 1). The ability of sulfobetaine polymers to permeate HepG2 MCTSs was analyzed.

Materials and methods

Materials

2,2′-Azobis[2-(2-imidazolin-2-yl)propane] and 2-(1-isobutyl) sulfanylthiocarbonylsulfanyl-2-methyl propionic acid were purchased from FUJIFILM Wako Pure Chemical Corporation (Osaka, Japan). [2-(Methacryloyloxy)ethyl]dimethyl-(3-sulfopropyl)ammonium hydroxide (MASB) and fluorescein *O*-methacrylate were purchased from Sigma–Aldrich, Japan (Tokyo, Japan). Other chemicals including 3-((3-methacrylamidopropyl) dimethylammonio)propane-1-sulfonate (MAAmSB) were purchased from Tokyo Chemical

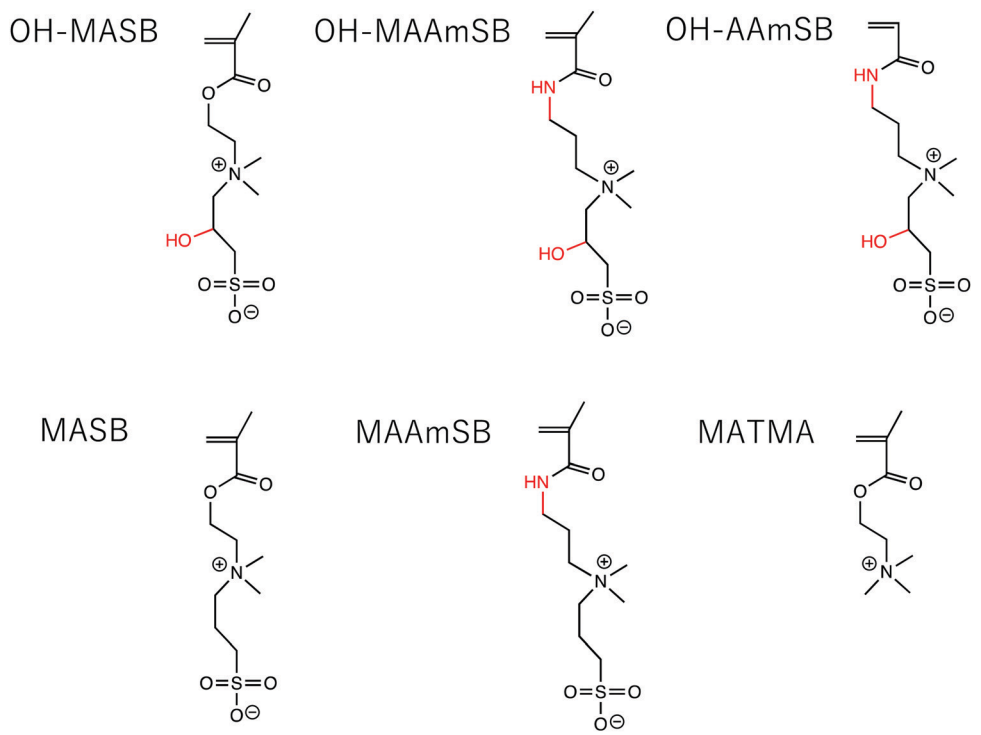

Fig. 1 Chemical structure of monomers used in this study.

Institute (TCI Co., Tokyo, Japan) and were used without further purification. HepG2 cells were purchased from the Cell Resource Center for Biomedical Research Institute of Development, Aging and Cancer, Tohoku University. NAP-25 column was purchased from GE Health care (Chicago, IL). P(MASB-*co*-PEGMA) was used as prepared in our previous study.[33]

Synthesis of 2-hydroxy-3-((2-methacryloyloxyethyl) dimethylammonio)propane-1-sulfonate (OH–MASB)

Sodium-3-chloro-2-hydroxypropanesulfonate (1.0 equiv., 60 mmol) and potassium iodide (0.035 equiv., 2.1 mmol) were dissolved in water. 2-Dimethylaminoethylmethacrylate (1.0 equiv., 60 mmol) in 2-propanol was added dropwise to the mixture and allowed to react for 18 h at 75 °C. After the reaction the solvent was removed, and hot ethanol (50 °C) was added to remove the insoluble salt. The resulting solution was concentrated and reprecipitated in diethyl ether and dried *in vacuo* overnight. Yield: 56.6%. ^{1}H NMR (in D_2O): δ (ppm) = 6.15 (s, 1H: C(CH_3)(=CH_2)–C(=O)O–, *cis*), 5.76 (s, 1H: C(CH)$_3$(=CH_2)–C(=O)O–, *trans*), 4.64 (d, 2H: –C(=O)OCH_2CH_2N + (CH_3)$_2CH_2$–), 4.34 (m, 1H: –CH_2CH(OH)CH_2SO_3–), 3.92 (d, 2H, –C(=O)O–CH_2CH_2N + (CH_3)$_2CH_2$–), 3.28 (d, 6H: –CH_2CH_2N + (CH_3)$_2CH_2$–), 1.92 (s, 3H,α-methyl C(CH_3)(=CH_2)–C(=O)O–). ESI: $[M + Na]^+$ = 318.1, $[M + K]^+$ = 334.1.

Synthesis of 2-hydroxy-3-((3-methacrylamidopropyl) dimethylammonio)propane-1-sulfonate (OH–MAAmSB)

Sodium-3-chloro-2-hydroxypropanesulfonate (1.0 equiv., 60 mmol) and potassium iodide (0.035 equiv., 2.1 mmol) were dissolved in water. *N*-(3-Dimethylaminopropyl)methacrylamide (1.0 equiv., 60 mmol) in 2-propanol was added dropwise to the mixture and allowed to react for 18 h at 75 °C. After the reaction the solvent was removed, and hot ethanol (50 °C) was added to remove the insoluble salt. The resulting solution was concentrated, reprecipitated in tetrahydrofuran and dried *in vacuo* for 3 days. Yield: 66.5%. ^{1}H NMR (in D_2O, Fig. S1, ESI†): δ (ppm) = 5.56 (s, 1H: C(CH_3)(=*CH_2*)–C(=O)NH–, *cis*), 5.32 (m, 1H: C(CH)$_3$(=*CH_2*)–C(=O)NH–, *trans*), 4.51 (m 1H: –CH_2*CH*(OH)CH_2SO_3–), 3.22 (m, 2H, –NH*CH_2*CH_2CH_2N$^+$(CH_3)$_2$–), 3.28–3.53 (m, 4H: –*CH_2*N$^+$(CH_3)$_2$*CH_2*–), 3.04 (d, 6H: –CH_2CH_2N$^+$*(CH_3)$_2$*CH_2–), 3.00 (m, 2H: –CH(OH)*CH_2*SO_3), 1.93 (m, 2H: –NHCH_2*CH_2*CH_2N$^+$(CH_3)$_2$–), 1.78 (s, 3H,a-methyl C(*CH_3*)(=CH_2)–C(=O)NH–). ESI: $[M + H]^+$ = 309.1, $[M + Na]^+$ = 331.1.

Synthesis of 2-hydroxy-3-((3-acrylamidopropyl) dimethylammonio)propane-1-sulfonate (OH–AAmSB)

Sodium-3-chloro-2-hydroxypropanesulfonate (1.0 equiv., 60 mmol) and potassium iodide (0.035 equiv., 2.1 mmol) were dissolved in water. *N*-[3-(Dimethylamino)propyl]acrylamide (1.0 equiv., 60 mmol) in 2-propanol was added dropwise to the mixture and allowed to react for 18 h at 75 °C. After the reaction the solvent was removed, and hot ethanol (50 °C) was added to remove the insoluble salt. The resulting solution was concentrated and reprecipitated in tetrahydrofuran and dried *in vacuo* for 3 days. Yield: 56.3%. ^{1}H NMR (in D_2O, Fig. S1, ESI†): δ = 6.27 (m, 1H: CH_2(=*CH*)C(=O)NH–), 6.19 (m 1H: *CH_2*(=CH)C(=O)NH–, *cis*), 5.78 (m, 1H: *CH_2*(=CH)C(=O)NH-, *trans*), 3.43–3.66 (m, 4H: –*CH_2*N$^+$(CH_3)$_2$*CH_2*–), 3.38 (m, 2H, –NH*$CH_2CH_2CH_2$*N$^+$(CH_3)$_2$–), 3.20 (d, 6H: –CH_2CH_2N$^+$*(CH_3)$_2$* CH_2–), 3.15 (m, 2H: –CH(OH)*CH_2*SO_3), 2.08 (m, 2H: –NHCH_2*CH_2*CH_2N$^+$(CH_3)$_2$–). ESI: $[M + H]^+$ = 295.1, $[M + Na]^+$ = 317.1.

Synthesis of sulfobetaine polymers

Sulfobetaine homopolymers were synthesized by aqueous reversible addition–fragmentation chain transfer (RAFT) polymerization. Typically, the MASB monomer was dissolved in pure water, followed by the chain transfer agent (CTA), 4-(2-carboxyethylsulfanylthiocarbonyl)sulfanyl-4-cyanopentanoic acid. The initiator, 2,2′- azobis[2-(2-imidazolin-2-yl)propane] was dissolved in methanol and mixed with the monomer/CTA solution. The molar ratio of monomer to CTA and initiator was [monomer]:[CTA]:[initiator] = 100:1:0.3, and the final concentration of the monomer was set to 0.1 M. The solvent was a mixture of pure water and methanol at a volume ratio of 2:1. Nitrogen gas was bubbled for 30 min to remove dissolved oxygen, and the polymerization was carried out in an oil bath at 60 °C for 18 h. The polymer was purified by dialysis in pure water (MWCO = 3500) for 7 days to remove any unreacted monomer. The polymer powder was obtained by freeze-drying the purified solution. The molecular weight of the polymers was determined *via* gel permeation chromatography using a JASCO system (Tokyo, Japan) with TSKgel G3000PW$_{XL}$ and G4000PW$_{XL}$ columns (Tosoh Co. Tokyo, Japan). The eluent was aqueous $NaNO_3$ (400 mM) calibrated with PEG standards.

Fluorescein modification to the ω-end of the sulfobetaine polymers

The ω-terminus of the homopolymers was modified with fluorescein by a two-step reaction.[33] First, the trithiocarbonate group was converted to a thiol group *via* an aminolysis reaction. Sulfobetaine homopolymer (1.0 equiv.) was dissolved in MQ water at 10 mg mL^{-1}. *n*-Butylamine (100 equiv.) was added to the polymer solution and stirred for 2 h at r.t. to substitute the trithiocarbonate group with a thiol group. After 2 h, *n*-butylamine was removed by evaporation and then purified in a dialysis membrane bag (MWCO = 3500) for 4 days. The obtained polymer was dissolved in 50 mM phosphate buffer at pH 8.0, and fluorescein-*O*-methacrylate (3.0 equiv.) dissolved in dimethyl sulfoxide was added to the solution and stirred for 18 h at r.t. in the dark. The reaction mixture was purified on an NAP-25 column, and the product was obtained by lyophilization. The degree of fluorescein modification was calculated from the absorbance at 492 nm (ε = 67 100 M^{-1} cm^{-1}) (Table 1).

Dynamic light scattering (DLS) measurements

The size of the sulfobetaine polymers in pure water and phosphate buffered saline (PBS, pH 7.4) was evaluated by DLS on a spectrometer equipped with a Peltier temperature controller (Zetasizer Nano ZS, Malvern Instruments, Malvern, UK). The polymer solution (10 mg mL^{-1}) was dissolved in Milli-Q water and/or PBS and stored for 24 h before measurement. The polymer solution was passed through a PVDF filter (pore size:

Table 1 Characterization and solution properties of polymers

Polymer	M_n	M_w/M_n	% Fluorescein	Hydrodynamic radius[a] (nm)		ζ-potential[a] (mV)	
				In MQ	In PBS	In MQ	In PBS
P(OH–MASB)	7600	1.36	15.7	90.7 ± 35.1	9.0 ± 1.4	−19.6 ± 0.2	−1.7 ± 0.5
P(OH–MAAmSB)	8800	1.14	11.1	5.7 ± 1.1	5.0 ± 0.5	27.3 ± 2.3	−3.5 ± 2.9
P(OH–AAmSB)	7800	1.31	18.6	3.6 ± 0.6	3.4 ± 0.3	18.7 ± 1.2	−5.3 ± 1.9
P(MASB)	9300	1.27	15.0	4.4 ± 0.8	4.6 ± 0.3	−30.4 ± 15.0	−0.3 ± 2.3
P(MAAmSB)	8500	1.24	14.4	8.8 ± 1.7	8.1 ± 1.6	6.6 ± 1.0	−0.4 ± 3.0
P(MATMA)	6900	1.18	17.2	84.8 ± 27.6	6.8 ± 2.9	31.6 ± 0.6	5.2 ± 7.0

[a] [Polymer] = 10 g L^{-1}.

0.45 μm) before the measurements were taken. The DLS measurements were performed at 25 °C with a wavelength of 632.8 nm and a 173° detection angle. The hydrodynamic diameter was determined using a Laplace inversion program (CONTIN).

Zeta-potential measurements

Zeta-potential measurements of the obtained polymers were performed at 25 °C by an electrophoretic light scattering analyzer (SZ-100, HORIBA) using a disposable cell equipped with a carbon electrode. The polymer solution (10 mg mL^{-1}) was dissolved in Milli-Q water and/or PBS and stored for 24 h before measurements.

Turbidity measurements

The turbidity of the polymer solutions was monitored on a UV-Vis spectrometer (JASCO, Tokyo, Japan) at 550 nm. P(OH–MASB) was dissolved in water or PBS (10 mg mL^{-1}) and stored for 24 h at r.t. The polymer solution was warmed up to 75 °C and equilibrated for 10 min. Transparency of the polymer solution was monitored in the cooling process from 75 °C to 5 °C at the cooling rate of 1.0 °C min^{-1}.

Cell viability of monolayer cultured cells

HepG2 cells were seeded at a concentration of 1×10^5 cells per mL. After preincubation in D-MEM buffer containing 10% FBS for 24 h at 37 °C containing 5% CO_2, polymer solution (< 4.0 mg mL^{-1}) was added and incubated for another 24 h. The cytotoxicity of the sulfobetaine polymers was evaluated using a cytotoxicity LDH Assay Kit-WST (Dojindo, Kumamoto, Japan). The activity of the lactate dehydrogenase released from damaged cells was evaluated in comparison to that released from nontreated cells and cells fully damaged by a surfactant.

Internalization of sulfobetaine polymers into monolayer cultured HepG2 cells

HepG2 cells (5.0×10^4 cells per mL) were preincubated on glass-bottom dishes for 24 h. The sulfobetaine polymer (final concentration: 1.0 mg mL^{-1}) in PBS was added to HepG2 cells in the presence of serum and incubated for 10 min at 37 °C containing 5% CO_2. After incubation, the glass-bottom dish was washed with PBS twice and immediately observed by confocal laser scanning microscopy (CLSM, FV-1000, Olympus, Tokyo, Japan).

Flow cytometry

HepG2 cells were preincubated at 50 000 cells in a 24-well microplate for 24 h. Fluorescein-modified polymers were added to the monolayer cultured cells at the final concentration ranging from 0.01 to 0.1 mg mL^{-1}, and cells were incubated in DMEM containing 10% FBS for another 10 min at 4 or 37 °C. After incubation, the cells were washed twice with cold PBS and trypsinized. Cells were harvested and centrifuged at 1800 rpm for 5 min. Trypsin was removed and the cell pellet was suspended with cold PBS. Flow cytometry was performed using a CytoFLEX flow cytometer (Beckman Coulter, Inc.) equipped with a 488 nm argon laser. Signals from the FL1 bandpass emission (530/30) were used to analyze 5000 events for each sample.

Preparation of HepG2 MCTS

HepG2 cells were dispersed in a U-bottom 96-well plate with a low protein adhesion surface (Prime Surface, Sumitomo Bakelite Co. Ltd., Tokyo, Japan) at a concentration of 1500 cells per well. The cells were cultured for 4 days at 37 °C and under 5% CO_2. The diameters of the obtained cells were calculated from microscopic images of 100 spheroids using ImageJ 1.50i.19,20 E.

Permeability into HepG2 MCTS

The HepG2 MCTSs were transferred into glass-bottom dishes. The dishes were placed on a CLSM, and the sulfobetaine polymer (final concentration: 1.0 mg mL^{-1}) was added to the spheroids in D-MEM containing 10% FBS. The permeation of fluorescein-labeled sulfobetaine was monitored every 1 min as the spheroids changed; this experiment used CLSM (FV-1000 Olympus) at 20 °C. The sliced images of the spheroids were obtained at 50 μm from the bottom of the spheroids. The line profiles of the intensity changes were analyzed using Olympus cellSens software, Ver. 3.1. Sliced images of the spheroids were obtained after 30 min of P(OH–MAAmSB) addition and included every 10 μm step from the bottom of the spheroids.

Live/Dead staining of HepG2 MCTS

The distribution of live and dead cells in HepG2 MCTS was observed after coincubation with the polymers (final concentration: 1.0 mg mL^{-1}) for 24 h. The cells in MCTS were stained using Live/Dead Cell Staining Kit II (PromoCell GmbH, Heidelberg, Germany) for 60 min, and fluorescence images were obtained by CLSM.

Estimation of lipophilicity and water solubility

The lipophilicity of monomers was estimated as *n*-octanol/water partition coefficients ($\log P_{o/w}$) using the SwissADME webtool.[37] XLOGP3 and iLOGP calculations were applied as the $\log P_{o/w}$; XLOGP3 is an atomistic method that includes correction factors and a knowledge base library, and iLOGP calculates the free energy of solvation in *n*-octanol and water using generalized Born (GB) parameters and the solvent accessible surface area (SASA).[38] The water solubility was calculated by ESOL, a simple calculation method that considers $\log P_{octanol}$, molecular weight, proportion of heavy atoms in aromatic systems, and number of rotational bonds to be important factors.[39]

High performance CLSM

High-resolution time-lapse imaging of MCTS was performed by FV-3000 (Olympus) using a resonant scan with a 30× silicone immersion objective. The refractive index of silicone oil is close to that of living tissue, enabling high-resolution observation deep inside the MCTSs with minimal spherical aberration. The images were taken every 1 s with a resolution of 512 × 512 pixels and the line profiles of a sliced depth and the mean fluorescence intensity of the divided regions were analyzed by Olympus cellSens software, Ver. 3.1.

Results

Polymer synthesis

In this study, we prepared 6 polymers: 5 sulfobetaine polymers and a cationic polymer as the comparison. The 5 sulfobetaine polymers were classified as methacrylate or (meth)acrylamide, with or without hydroxy groups in between the zwitterions. An OH group containing three monomers, OH–MASB, OH–MAAmSB, and OH–AAmSB, was synthesized by the method betaine surfactant synthesis described by Yan *et al.*[40] All polymers were obtained by using aqueous RAFT polymerization and were found to have a molecular weight of approximately 8000 with a relatively narrow distribution (1.14–1.36) (Table 1 and Fig. S3, ESI†). For cell observation, fluorescein was substituted at the ω-end of sulfobetaine polymers by a 2-step reaction: conversion of the trithiocarbonate group as a chain transfer agent to a thiol using an aminolysis reaction followed by a Michael addition reaction with fluorescein methacrylate in the presence of a reducing agent.

Solution properties of sulfobetaine polymers

First, DLS measurements were performed in pure water and in PBS at 25 °C. The results are shown in Table 1. In pure water, all sulfobetaine polymers except P(OH–MASB) showed a hydrodynamic radius of less than 10 nm, which indicated high solubility in pure water (Fig. 2a). P(OH–MASB) showed a hydrodynamic radius of ∼90 nm. In PBS, the hydrodynamic radii of the polymers in all polymer solution were less than 10 nm, including P(OH–MASB). The aggregated P(OH–MASB) mostly dissociated into single molecules in the presence of salt. These results indicated that the polymer was in the aggregated state found at the upper critical solution temperature (UCST). Turbidity measurements were performed on P(OH–MASB) during the cooling process. As shown in Fig. 2b, the P(OH–MASB) solution showed a broad UCST-type transition from ∼60 °C to ∼20 °C in pure water. The transparent solution was also found for the temperature range in PBS. The behavior is similar to that shown in P(MASB) which has a higher molecular weight than the polymers applied in this study.[23] Then, the zeta-potential of the sulfobetaine polymers was also measured in pure water and in PBS (Table 1). Sulfobetaine polymers are supposed to have neutral or slightly negative values; however, interesting results were obtained in pure water. P(OH–MASB) had a negative value (−19.6 ± 0.2 mV), which was likely due to the formation of microspheres.[41] The negative charge was removed by the dissociation of microspheres in the presence of salt. In contrast, the (meth)acrylamide polymers showed positive values. The zeta-potential of P(OH–MAAmSB) was highest with a value of +27.3 ± 2.3 mV. These polymers did not associate intermolecularly to form microspheres. However, the positive charges of the sulfobetaine polymers were also canceled out, leaving a slightly negative charge in the PBS. The results implied that the OH-side groups inhibited the intermolecular dipole–dipole interactions and supported the formation of an inner salt in a sulfobetaine side chain.

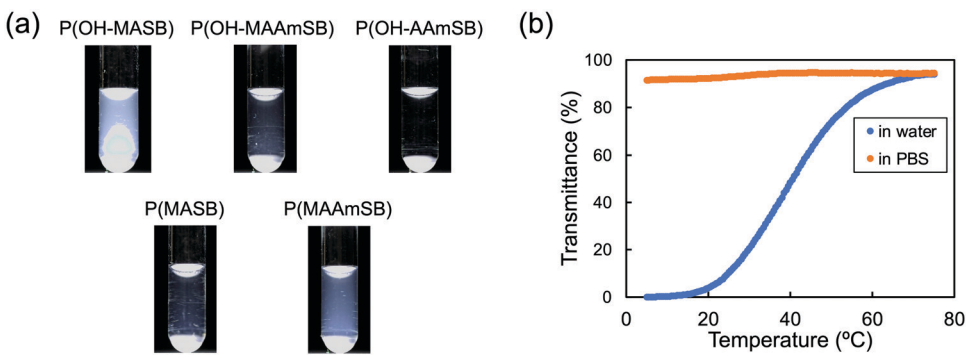

Fig. 2 (a) Photo images of sulfobetaine polymer solutions in water. (b) Transmittance of P(OH–MASB) solutions as a function of temperature. The cooling rate of the solutions was 1.0 °C min^{-1}. [Polymer] = 10 g L^{-1}.

Cell viability and membrane translocation of sulfobetaine polymers against monolayer cultured cells

The cytotoxicity of the sulfobetaine polymers was evaluated using human hepatoma HepG2 cells. The sulfobetaine polymers were added to the HepG2 cells and incubated for another 24 h. As shown in Fig. 3, the sulfobetaine polymers showed little cytotoxicity. No significant decrease in cell viability was detected for P(OH–MAAmSB) and P(OH–AAmSB), and a less than 5% decrease in viability was observed with P(MASB), P(MAAmSB), and P(OH–MASB) at 2.0 mg mL^{-1}, the highest concentration. However, P(MATMA), the positively charged polymer, decreased cell viability as its concentration increased. The decrease in cell viability might be due to membrane disruption by the cationic polymer. The disruption of HeLa cell membranes was confirmed by the release of hydrolyzed calcein-AM from the cytosol.[33] Next, fluorescein modified sulfobetaine polymers were added to HepG2 cells in the presence of serum and incubated for 10 min at 37 °C. All the sulfobetaine polymers except P(OH–MASB) were observed in HepG2 cells (Fig. 4). Although a slightly high intensity was confirmed in mitochondria, fluorescence was observed in entire cells containing nuclei. The fast translocation and distribution behavior in cells indicated that these sulfobetaine polymers were internalized into cells by membrane translocation as shown in our previous studies.[33,42] P(OH–MASB) could not internalize in HepG2 cells under the observation conditions. Some of the polymers were found in different conditions. The P(OH–MASB) in the cell culture medium was a slightly turbid solution that might have formed aggregates and affected internalization into cells. In contrast, cationic P(MATMA) also showed internalization in the cells. There were large differences in the fluorescence intensity between the cells, indicating that internalization might be an effect of membrane disruption. Next, the cellular uptake behavior of the polymers was compared after 10 min incubation by flow cytometry measurements (Fig. S4, ESI†). For all polymers, the fluorescence intensities from the cells were increased by increasing the concentration. However, the mean fluorescence intensities of sulfobetaine polymers were higher than that of P(MATMA) under each condition. Interestingly, (meth)acrylamide sulfobetaine polymers showed a significant increase at 4 °C. There are differences between the (meth)acrylamides, and P(OH–MAAmSB) showed the highest effect. Therefore, the difference in the fluorescence intensity at the higher concentration and at 4 °C might reflect the rate of membrane translocation and capacity of cellular uptake against the polymers. On the other hand, the P(MATMA) decreased the fluorescence intensity by incubation at 4 °C. The results indicated that the P(MATMA) internalized in cells by membrane disruption and/or endocytotic pathway.

Permeation of sulfobetaine polymers into MCTS

Based on the results of monolayer cultured cells, sulfobetaine polymers were evaluated for permeation behaviors into HepG2 MCTSs. HepG2 MCTSs were prepared from 1500 cells and incubated in U-shaped 96-well plates for 4 days at 37 °C, 5% CO_2. The obtained spheroids were 325 ± 31 μm in diameter. Sulfobetaine polymers were added to the spheroids in serum-containing media and time-lapse observation was performed using CLSM to evaluate the permeation of sulfobetaine polymers into MCTSs. Here, the depth was ~50 μm from the bottom of the MCTSs; therefore, the obtained image appears smaller than the calculated image. The results are shown in Fig. 5. P(MASB) is a representative sulfobetaine polymer, and we have also been studying cellular membrane translocation using this homopolymer and its copolymer. P(MASB-*co*-PEGMA), which contains 2.5 mol% PEGMA in the copolymer, exhibited superior permeation into human glioblastoma MCTS after conjugation with doxorubicin, an anticancer drug.[35] As a result, P(MASB) also gradually permeated the HepG2 spheroid from the periphery to the center. The fluorescence of P(MASB) was observed in the periphery of the MCTS at 3 min after the addition and increased the intensity around the area as time proceeded. However, little fluorescence was detected from the center of the MCTS within this time range (~20 min). Similar behavior of P(MASB) permeation was observed in P(OH–MASB). Line profiles of the permeation behaviors are depicted in these images (Fig. 6). The permeation behavior of cationic P(MATMA)

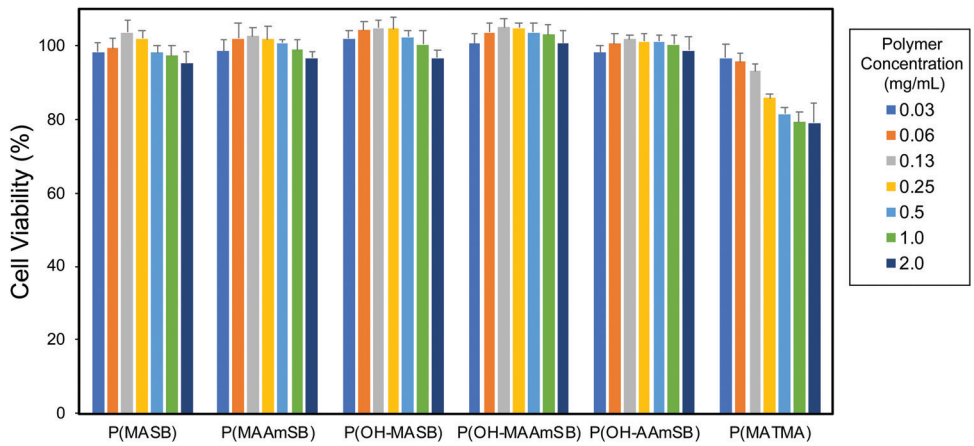

Fig. 3 Viability of HepG2 cell after 24 h coincubation with polymer at 37 °C, 5% CO_2.

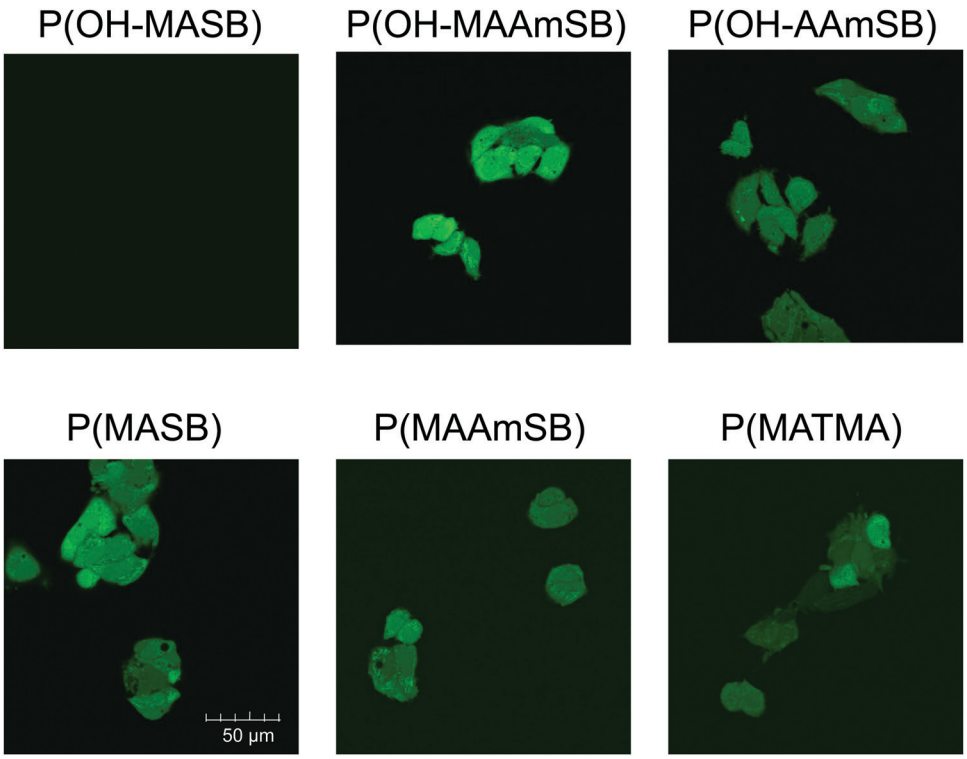

Fig. 4 Internalization of fluorescein modified polymers into monolayer cultured HepG2 cells after 10 min incubation at 37 °C, 5% CO_2.

seemed similar, but not identical to that of P(MASB). The fluorescence intensity gradually increased in the periphery, although the permeation from outside the MCTS was limited to only the first layer. Even with the increasing intensity of the baseline, outside of the spheroid, the intensity of the center did not increase on this time scale. (Meth)acrylamide sulfobetaine polymers had a faster and stronger fluorescence intensity in the MCTSs than the methacrylate polymers. In particular, P(OH–MAAmSB) showed the best permeation performance. The P(OH–MAAmSB) propagated acutely to the center of the MCTS. At the sliced depth, the polymer reached to the center region, and the fluorescence intensity increased continuously. The fluorescence intensity was apparently higher than the baseline intensity. The P(OH–MAAmSB) was membrane translocated and accumulated in the peripheral of MCTS, followed by diffusion and permeation to the center of the MCTS.[43] Overall, P(OH–MAAmSB), the methacrylamide sulfobetaine polymer with an OH-side group, permeated the MCTSs the most quickly and effectively.

Live/dead assay of sulfobetaine polymer added MCTS

Live/dead cells in the MCTS were observed using calcein-AM/ethidium homodimer III staining of the MCTS after coincubation with polymers for 24 h (Fig. S5, ESI†). Here, the MCTS was observed at the same depth, 50 μm from the bottom (Fig. S6, ESI†), as that used in the permeation studies as mentioned above. The concentration of polymers was fixed at 1.0 mg mL^{-1}, which is also the same condition as was used in the permeation study and the experiments on the cytotoxicity of the sulfobetaine polymers in terms of concentration. As shown in Fig. S5 (ESI†), most cells were alive except for a few cells around the periphery of the MCTSs on sulfobetaine polymers. More dead cells were observed on the addition of cationic P(MATMA), which was ~80% viable in the monolayer culture. The dead cells were distributed evenly throughout the center of the MCTS. Although, HepG2 MCTSs have been reported to have an 8.5-fold increase in the IC_{50} value against an anticancer drug compared to that of monolayer culture.[44] The results indicated that concentrated P(MATMA) at the surface of cell in the periphery of each spheroid gradually permeated into the center of the spheroid by disruption of the MCTS cell membranes.

Discussion

Estimation of partition coefficient for sulfobetaine monomers

To elucidate the difference in efficiency of permeation of the MCTSs by the sulfobetaine polymers, the solubility in aqueous media was investigated at the monomer level. First, the *n*-octanol/water partition coefficient of the monomers was estimated. As shown in Table 2, the coefficients were calculated by two methods: XLOGP3 and iLOGP. Both calculation results for the monomers indicated that most of the monomers were partitioned into the water layer. In particular, negative values were obtained by XLOGP3 calculation for OH–sulfobetaines. These results indicate that the OH–sulfobetaines are more soluble and more likely to preferably partition into the water layer than other sulfobetaines that do not have OH-side groups. ESOL calculations of the OH–sulfobetaines were also indicated that they are more

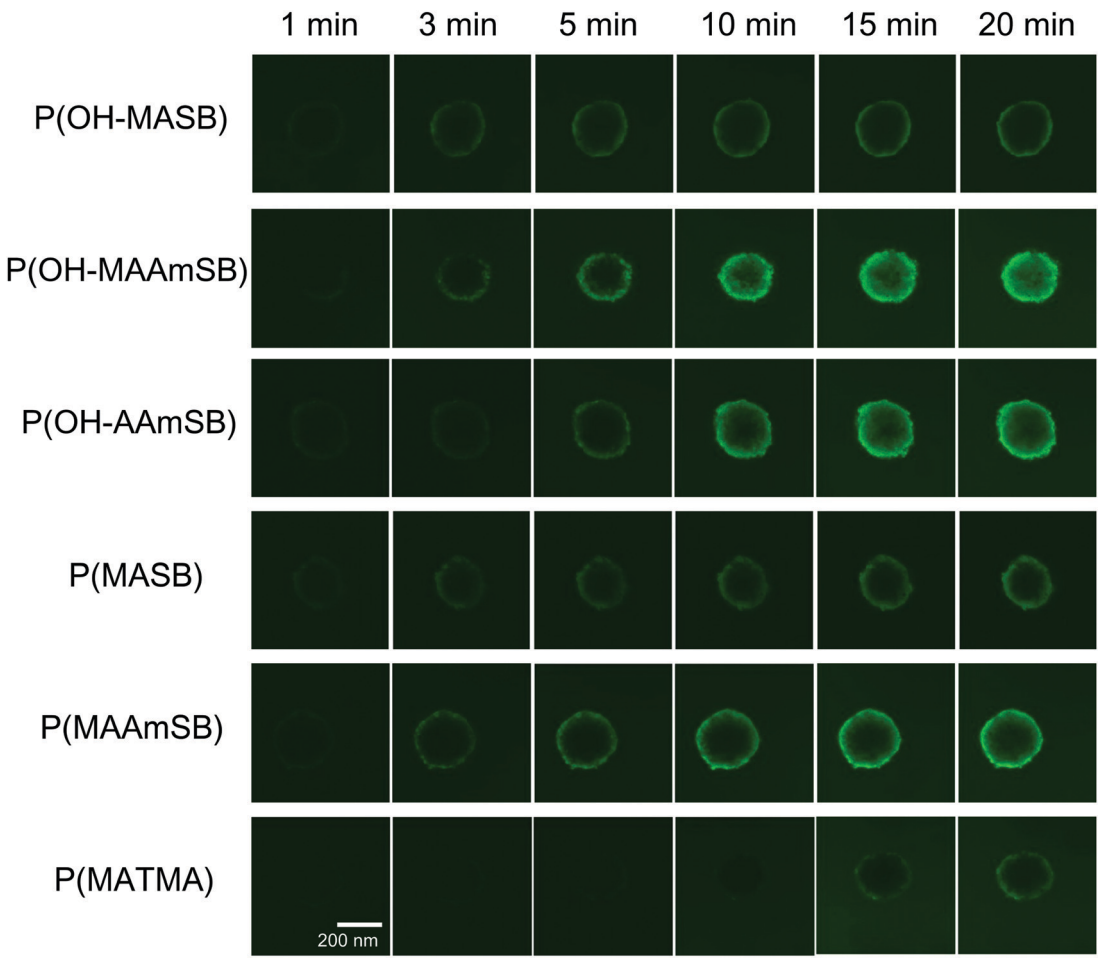

Fig. 5 Permeation of polymers into HepG2 MCTS in the presence of serum. Fluorescence images were captured by CLSM at 50 μm from the bottom of MCTS. [Polymer] = 1.0 g L^{-1}.

soluble in water. In particular, the (meth)acrylamide polymers showed higher values than that of the methacrylate. Additionally, the *n*-octanol/water partition coefficient ($\log P_{o/w}$) was calculated by iLOGP, which considers the free energy of solvent molecules. The $\log P_{O/W}$ of methanol was 0.81, although the sulfobetaine monomers showed the negative values. The OH–MAAmSB had quite a small $\log P_{o/w}$ (−8.24). The high water solubility of P(OH–MAAmSB) could be inherited from the characteristics of the monomer OH–MAAmSB and would also have a correlation with the excellent permeability into MCTS. As shown in Table 1, the size and zeta potential measurements of (meth)acrylamide sulfobetaine polymers in pure water indicated that the polymers were positively charged at the single chain level, and the positive charge increased with the number of hydroxyl groups. Such a positive charge can enhance the interaction with a negatively charged cellular membrane.

In our previous report, we proposed the mechanism for membrane translocation that inner salts of zwitterions form a six-membered ring-like conformation and interact with phospholipids to form 'a double' bilayer membrane to internalize into cells. Here, the presence of the hydroxy group in the sulfobetaine polymer might stabilize the formation of inner salts, which have a six-membered ring-like structure. During the membrane translocation, the side chains dynamically form the inner salts and/or interact with phospholipids by dipole–dipole interaction, resulting in a slightly hydrophobic effect. The presence of hydroxyl groups could affect the hydrophilicity and assist smooth translocation to cells. And the accumulated polymer in the peripheral cells of MCTS permeates to the center with the concentration dependency.

Detailed analysis of permeation behavior

To analyze the details of P(OH–MAAmSB) permeation into MCTS, high-performance CLSM was performed for time-lapse observations (Fig. 7, ESI†: ×10 speed). Interestingly, P(OH–MAAmSB) was first distributed around the intercellular space, gradually increasing the fluorescence intensity. These phenomena were observed from 30 s, and this behavior was also confirmed by the spikes in the line profile depicted in the fluorescence images. Following distribution in intercellular space, membrane translocation of P(OH–MAAmSB) was observed from the periphery of the MCTSs at approximately 100 s. Membrane-translocated P(OH–MAAmSB) diffused uniformly throughout the cells at the periphery of the MCTSs. Once P(OH–MAAmSB) was poured into

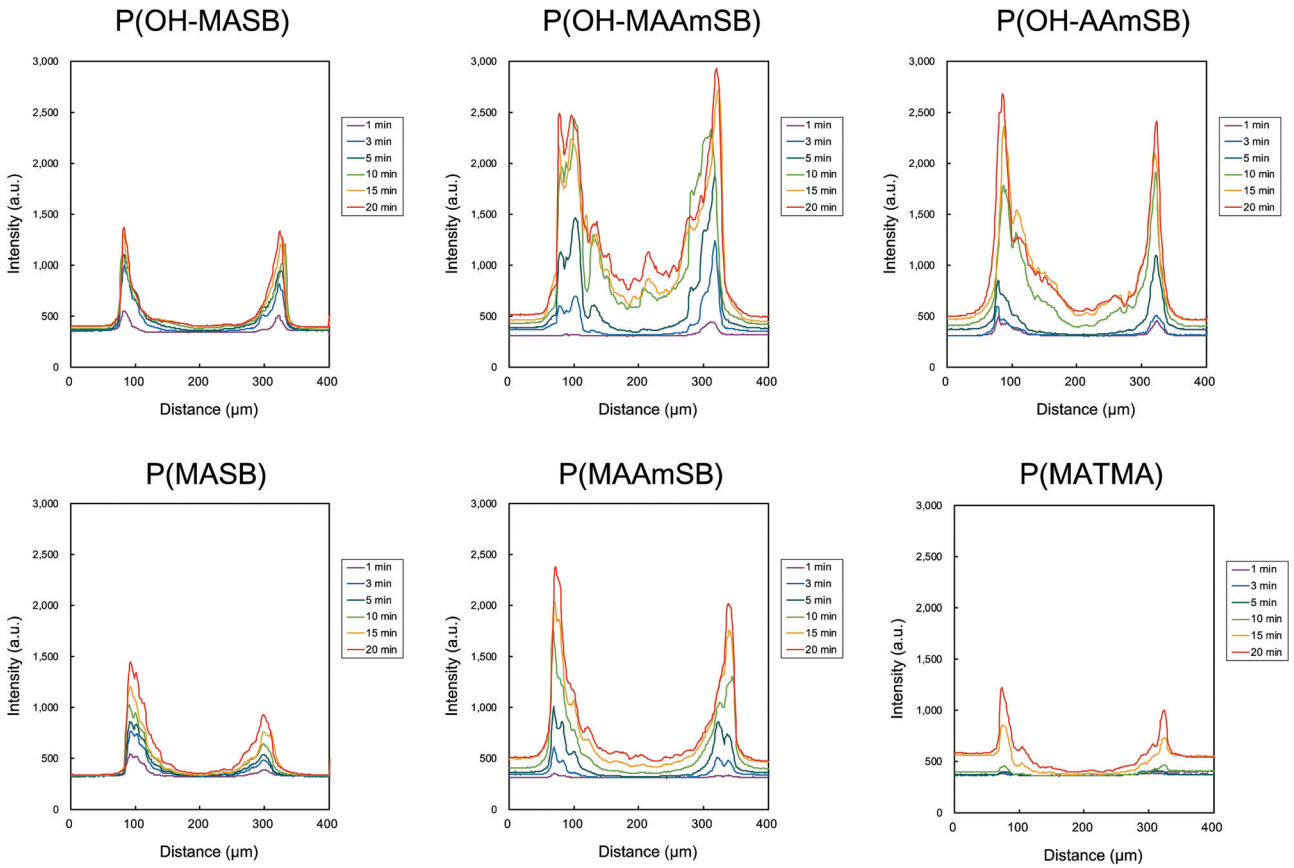

Fig. 6 Line profiles of fluorescence intensity from the polymers permeated into MCTS. The profiles were depicted from Fig. 5.

Table 2 Calculated log $P_{O/W}$ and the log S values of monomers

Monomer	Polymerizable group	Hydroxy group	log $P_{O/W}$ iLOGP	log $P_{O/W}$ XLOGP3	log S ESOL
OH–MASB	MA	(+)	−3.37	−0.60	−0.70
OH–MAAmSB	MAAm	(+)	−8.24	−0.82	−0.58
OH–AAmSB	AAm	(+)	−2.80	−1.19	−0.26
MASB	MA	(−)	−3.01	0.38	−1.22
MAAmSB	MAAm	(−)	−3.13	0.16	−1.09
MATMA	MA	(−)	−1.03	1.21	−1.34
SPMA	MA	(−)	0.84	0.04	−0.73

the cells, the fluorescence intensity increased in each cell. The P(OH–MAAmSB) gradually propagated toward the center to the neighboring cells, although the exact direction was difficult to predict. One of the reasons for this difficulty is that three-dimensional information could not be determined during this experiment. The MCTS was concentrically divided into 6 regions from the outside to the center and analyzed the mean fluorescence intensity of each area as a function of time (Fig. 7c and d). After increasing the outside of the MCTS (ROI(5–6)), other regions were increased their intensity. The increase of intensity was faster farther from the center, located in the peripheral of the MCTS. After the equilibration of the ROI(5–6) area, outside MCTS, the polymer permeated into the inside areas of MCTS. In the case of ROI(1), the center region of MCTS, there was an inflection point at around 150 s, followed by linearly increased intensity from ∼ 200 s to ∼ 500 s. The behavior indicated that the initial slow curve could be assigned to the increase of intercellular space, and the linear increase could be the permeation of P(OH–MAAmSB) into the center of MCTS. We have many findings about P(MASB-*co*-PEGMA), therefore we also observed the copolymer for comparison (Fig. S7, ESI†). The copolymer was also first distributed in the intercellular space of the MCTSs. The time scale of the distribution was ∼10-fold slower than that of P(OH–MAAmSB), and the fluorescence intensity remained weak, and permeation into cells in the MCTSs was not observed on this time scale. This difference in the permeation of the MCTSs by P(OH–MAAmSB) and P(MASB-*co*-PEGMA) does not necessarily correlate with the membrane permeability of the monolayer culture cells.

Finally, based on the findings in this study, we propose membrane translocation for the enhancement of MCTS permeability of P(OH–MAAmSB) as in Fig. 8. The (meth)acrylamide main chain and the formation of the inner salts in the side chain were indicated to play the key roles; (i) inner salt of P(OH–MAAmSB), which had a positive charge in pure water, dynamically changes the conformation and enhances the accumulation to the vicinity of the negatively charged cellular membrane; (ii) the hydroxy group between the zwitterion accelerates the membrane translocation to the inner aqueous phase; and (iii) as the result of highly concentrated P(OH–MAAmSB), the polymer permeates to the neighboring

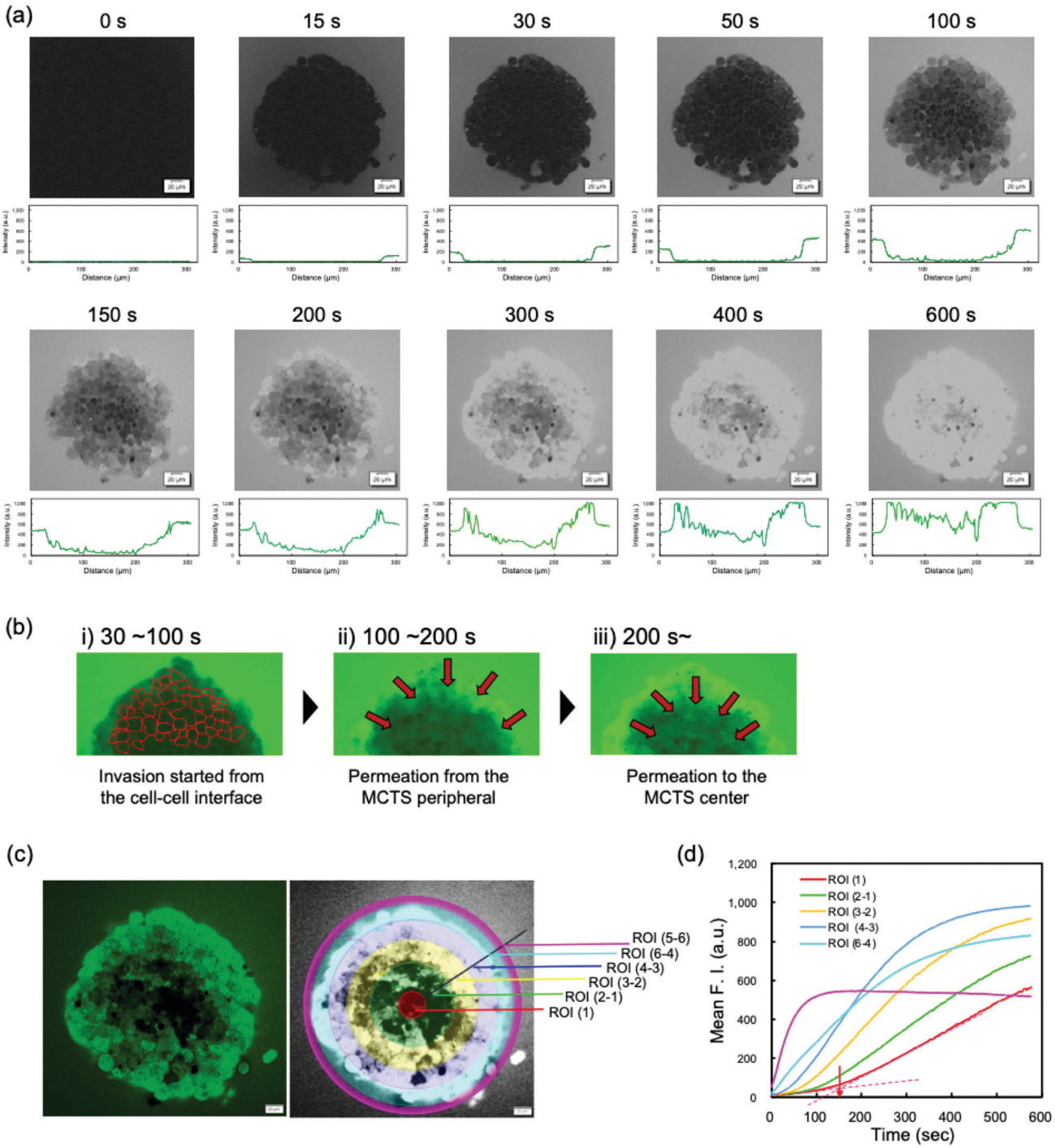

Fig. 7 (a) Time lapse images and the line profiles of P(OH–MAAmSB) added MCTS obtained by high performance-CLSM. (b) Schematic illustration of permeation behavior into MCTS. (c) CLSM image of P(OH–MAAmSB) added MCTS (left) and the divided areas for the analysis (right). (d) Time-lapse analysis of fluorescent intensity for P(OH–MAAmSB) in the divided areas of HepG2 MCTS. The red arrow indicates the time of permeation into the center area (ROI (1)) by P(OH–MAAmSB).

cells by concentration dependency *via* direct membrane–membrane interaction.

The proposed mechanism can provide an idea for the further design of nanocarriers; in addition, evaluation of the permeation into MCTSs will be a key index for the development of nanocarriers.

Conclusions

In this study, we prepared sulfobetaine homopolymers from the monomers; to obtain MCTS permeable polymers, we focused on (i) polymerizable groups, and (ii) hydroxy groups between zwitterions, to obtain MCTS permeable polymers. The

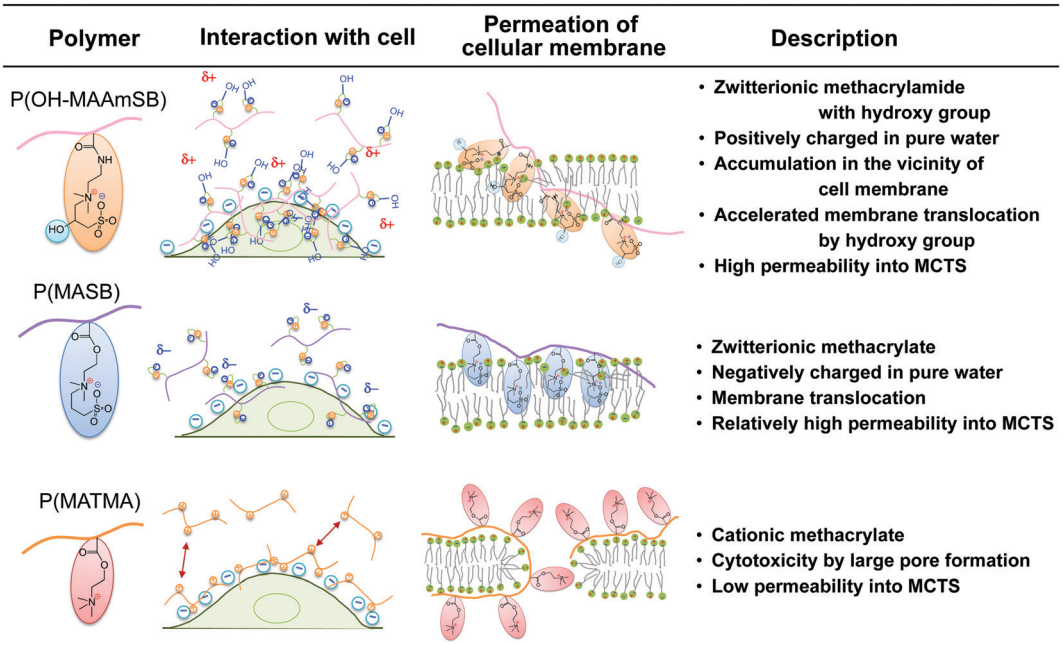

Fig. 8 Proposed mechanism of internalization into cells by the sulfobetaine polymers (P(OH–MAAmSB), P(MASB)) and the cationic polymer, P(MATMA).

(meth)acrylamide-type polymers, especially P(OH–MAAmSB), which also has a hydroxyl group in its side chain, can easily permeate MCTSs. In the presence of serum, P(OH–MAAmSB) could reach the center of an MCTS, ~325 μm in diameter, approximately 150 s after addition, and the amount of migration in the center could be increased. The monomer OH–MAAmSB was expected to have an extremely low log $P_{O/W}$ value. In addition, the positively charged zeta-potential of the polymer was considered to form inner salts in water. These features may have contributed to the excellent MCTS permeation; however, there is still room for improving our understanding of the MCTS permeability of P(OH–MAAmSB). The detailed analysis and newly designed sulfobetaine polymers might be applicable in the areas of drug screening, bioimaging, *etc.*

Conflicts of interest

There are no conflicts to declare.

Acknowledgements

This work was partly supported by the Cooperative Research Program (Joint Usage/Research Center program) of Institute for Frontier Life and Medical Sciences, Kyoto University, Japan-Korea Basic Scientific Cooperation Program between JSPS and NRF (JPJSBP120208802), the International Cooperation Program managed by the National Research Foundation of Korea (NRF-2020K2A9A2A08000126), and the JSPS KAKENHI Grant-in-Aid for Scientific Research (B) 21H03814.

References

1 H. Sung, J. Ferlay, R. L. Siegel, M. Laversanne, I. Soerjomataram, A. Jemal and F. Bray, *Ca-Cancer J. Clin.*, 2021, **71**, 209–249.
2 M. Gerlinger, A. J. Rowan, S. Horswell, M. Math, J. Larkin, D. Endesfelder, E. Gronroos, P. Martinez, N. Matthews, A. Stewart, P. Tarpey, I. Varela, B. Phillimore, S. Begum, N. Q. McDonald, A. Butler, D. Jones, K. Raine, C. Latimer, C. R. Santos, M. Nohadani, A. C. Eklund, B. Spencer-Dene, G. Clark, L. Pickering, G. Stamp, M. Gore, Z. Szallasi, J. Downward, P. A. Futreal and C. Swanton, *N. Engl. J. Med.*, 2012, **366**, 883–892.
3 J. Zugazagoitia, C. Guedes, S. Ponce, I. Ferrer, S. Molina-Pinelo and L. Paz-Ares, *Clin. Ther.*, 2016, **38**, 1551–1566.
4 V. Schirrmacher, *Int. J. Oncol.*, 2019, **54**, 407–419.
5 J. Rodrigues, M. A. Heinrich, L. M. Teixeira and J. Prakash, *Trends Cancer Res.*, 2021, **7**, 249–264.
6 T. Wang, L. Wang, G. Wang and Y. Zhuang, *Bioresour. Bioprocess*, 2020, **7**, 1–34.
7 R. Lama, L. Zhang, J. M. Naim, J. Williams, A. Zhou and B. Su, *Bioorg. Med. Chem.*, 2013, **21**, 922–931.
8 L. G. Griffith and M. A. Swartz, Capturing complex 3D tissue physiology in vitro, *Nat. Rev. Mol. Cell Biol.*, 2006, **7**, 211–224.
9 X. Cui, Y. Hartanto and H. Zhang, *J. R. Soc., Interface*, 2017, **14**, 20160877.
10 H. Shen, S. Cai, C. Wu, W. Yang, H. Yu and L. Liu, *Micromachines*, 2021, **12**, 96.
11 A. Kamatar, G. Gunay and H. Acar, *Polymers*, 2020, **12**, 2506.
12 M. E. Katt, A. L. Placone, A. D. Wong, Z. S. Xu and P. C. Searson, *Front. Bioeng. Biotechnol.*, 2016, **4**, 12.
13 H. Lu and M. H. Stenzel, *Small*, 2018, **14**, e1702858.
14 A. Tchoryk, V. Taresco, R. H. Argent, M. Ashford, P. R. Gellert, S. Stolnik, A. Grabowska and M. C. Garnett, *Bioconjugate Chem.*, 2019, **30**, 1371–1384.
15 M. Millard, I. Yakavets, V. Zorin, A. Kulmukhamedova, S. Marchal and L. Bezdetnaya, *Int. J. Nanomed.*, 2017, **12**, 7993–8007.
16 L. D. Blackman, P. A. Gunatillake, P. Cass and K. E. S. Locock, *Chem. Soc. Rev.*, 2019, **48**, 757–770.

17 A. Laschewsky, *Polymers*, 2014, **6**, 1544–1601.
18 A. B. Lowe and C. L. McCormick, *Chem. Rev.*, 2002, **102**, 4177–4189.
19 J. Baggerman, M. M. J. Smulders and H. Zuilhof, *Langmuir*, 2019, **35**, 1072–1084.
20 A. Venault and Y. Chang, *Langmuir*, 2019, **35**, 1714–1726.
21 M. He, K. Gao, L. Zhou, Z. Jiao, M. Wu, J. Cao, X. You, Z. Cai, Y. Su and Z. Jiang, *Acta Biomater.*, 2016, **40**, 142–152.
22 J. Seuring and S. Agarwal, *Macromol. Rapid Commun.*, 2012, **33**, 1898–1920.
23 N. M. Nizardo, D. Schanzenbach, E. Schönemann and A. Laschewsky, *Polymers*, 2018, **10**, 325.
24 J. Niskanen and H. Tenhu, *Polym. Chem.*, 2016, **8**, 220–232.
25 N. Wang, B. T. Seymour, E. M. Lewoczko, E. W. Kent, M.-L. Chen, J.-H. Wang and B. Zhao, *Polym. Chem.*, 2018, **9**, 5257–5261.
26 E. M. Lewoczko, N. Wang, C. E. Lundberg, M. T. Kelly, E. W. Kent, T. Wu, M.-L. Chen, J.-H. Wang and B. Zhao, *ACS Appl. Polym. Mater.*, 2021, **3**, 867–878.
27 V. A. Vasantha, C. Junhui, T. B. Ying and A. Parthiban, Salt-Responsive Polysulfobetaines from Acrylate and Acrylamide Precursors: Robust Stabilization of Metal Nanoparticles in Hyposalinity and Hypersalinity, *Langmuir*, 2015, **31**(40), 11124–11134.
28 M. Sponchioni, P. Rodrigues Bassam, D. Moscatelli, P. Arosio and U. Capasso Palmiero, Biodegradable Zwitterionic Nanoparticles with Tunable UCST-Type Phase Separation under Physiological Conditions, *Nanoscale*, 2019, **11**(35), 16582–16591.
29 N. Morimoto and M. Yamamoto, Design of an LCST-UCST-Like Thermoresponsive Zwitterionic Copolymer, *Langmuir*, 2021, **37**(11), 3261–3269.
30 N. Morimoto, Y. Oishi and M. Yamamoto, *Macromol. Chem. Phys.*, 2020, **221**, 1900429.
31 V. Hildebrand, A. Laschewsky and E. Wischerhoff, *Polym. Chem.*, 2016, **7**, 731–740.
32 V. Arjunan Vasantha, A. Oh Biying and A. Parthiban, *J. Appl. Polym. Sci.*, 2018, **135**, 46178.
33 N. Morimoto, M. Wakamura, K. Muramatsu, S. Toita, M. Nakayama, W. Shoji, M. Suzuki and F. M. Winnik, *Biomacromolecules*, 2016, **17**, 1523–1535.
34 N. Morimoto, R. Takei, M. Wakamura, Y. Oishi, M. Nakayama, M. Suzuki, M. Yamamoto and F. M. Winnik, *Sci. Rep.*, 2018, **8**, 1128.
35 N. Morimoto and M. Yamamoto, *Biomacromolecules*, 2020, **21**, 5044–5052.
36 T. Goda, H. Hatano, M. Yamamoto, Y. Miyahara and N. Morimoto, *Langmuir*, 2020, **36**, 9977–9984.
37 A. Daina, O. Michielin and V. Zoete, *Sci. Rep.*, 2017, **7**, 42717.
38 A. Daina, O. Michielin and V. Zoete, *J. Chem. Inf. Model.*, 2014, **54**, 3284–3301.
39 J. S. Delaney, *J. Chem. Inf. Comput. Sci.*, 2004, **44**, 1000–1005.
40 L. Yan, J. Ma, Z. Cui, J. Jiang, B. Song and X. Pei, *J. Surfactants Deterg.*, 2019, **22**, 47–60.
41 N. Morimoto, K. Muramatsu, S.-I. M. Nomura and M. Suzuki, *Colloids Surf., B*, 2015, **128**, 94–99.
42 N. Morimoto, Y. Oishi and M. Yamamoto, *Macromol. Biosci.*, 2020, **20**, e2000205.
43 T.-M. Achilli, S. McCalla, J. Meyer, A. Tripathi and J. R. Morgan, *Mol. Pharmaceutics*, 2014, **11**, 2071–2081.
44 A. Oshikata, T. Matsushita and R. Ueoka, *J. Biosci. Bioeng.*, 2011, **111**, 590–593.

